View metadata, citation and similar papers at core.ac.uk
brought to you by CORE
provided by CERN Document Server



# Synchrotron Tomography for the Study of Void Formation in Internal Tin $Nb_3Sn$ Superconductors

Astrid Haibel and Christian Scheuerlein

***Abstract*—Synchrotron absorption tomography has been applied for the study of voids formed during the thermal treatment of internal tin $Nb_3Sn$ strands. Possible void formation mechanisms and in particular the effect of Sn phase transformations and melting are discussed based on a quantitative void description. Sn melting changes mainly the shape and volume of the individual voids but does not increase the total void volume in the strand.**

***Index Terms*—Superconducting materials, tomography.**

## I. Introduction

DURING the thermal treatment of $Nb_3Sn$ superconducting (SC) strands, the formation of voids in the strand matrix is commonly observed [1]. Voids can be detrimental because they reduce the homogeneity of the strand chemistry and they can lead to localized stress conmentrations. Both effects may cause a degradation of the superconductor critical current. Therefore, it is desirable to avoid or at least to better control the void growth during the strand heat treatment, e.g., through optimized strand designs or heat treatment cycles.

In $Nb_3Sn$ strands that are produced by the internal tin process one can distinguish between at least two types of voids. One void type is formed during the Cu–Sn interdiffusion heat treatment at comparatively low temperatures in the diffusion centers of internal tin design strands. The cross section of these voids can approach that of an entire Sn pool and their formation is often ascribed to the Sn volume expansion upon melting. For the reaction, heat treatment of some strands holding steps below the Sn melting temperature are recommended in order to reduce the effect of Sn melting. The usefulness of such holding steps is discussed controversially [2].

A second type of voids observed in reacted $Nb_3Sn$ strands has comparatively small (about 1 $\mu m^2$) cross sections and is distributed around the SC filaments. The formation of these voids has been attributed to differences in the diffusion rates of Cu in Sn and Sn in Cu and/or to the different densities of the formed phases.

So far the void formation in $Nb_3Sn$ strands has been examined by metallographic techniques [3], which can not provide the three-dimensional shape of the voids and their distribution along the strand axis. Furthermore, since metallography is destructive the void formation process during a series of heat treatments can not be observed within the same sample. A further disadvantage when analyzing metallographic images is that artefacts, which may occur because of the sample preparation by mechanical grinding and polishing, can not always be excluded.

In order to overcome these experimental problems, 3-D tomograms of internal tin $Nb_3Sn$ strand samples after *ex-situ* thermal treatments have been reconstructed from the synchrotron radiation absorption contrast. Based on a quantitative void description obtained from these tomograms, the potential of synchrotron tomography for the study of voids in SC strands and the void formation mechanisms are discussed. Main subject of this article is the formation of the relatively large voids in the center of the Sn pools at heating temperatures up to 245 °C, just above the Sn melting temperature.

TABLE I
Relative Volume Fractions (vol.%) of the Individual Components in the Non-Reacted $Nb_3Sn$ Wire

| Material | Vol. % |
|---|---|
| Cu | 80.2 % |
| Nb-Ta filaments | 8.9 % |
| Sn pools | 5.6 % |
| Ta barrier | 1.8 % |
| Nb barrier | 3.5 % |

## II. Experimental

### A. Samples

The samples analyzed are $Nb_3Sn$ strands of the internal tin design, which are described in detail in [4]. The samples have been drawn down to a diameter of 0.684 mm. The strand comprises 19 diffusion centers, with 198 Nb–7.5wt.%Ta filaments (filament diameter about 3.4 $\mu$m) around each of the 19 main Sn pools, which have an approximate diameter of 40 $\mu$m. The filament spacing is less than 1 $\mu$m. The strand has a common diffusion barrier made of Nb and Ta. The relative volume fractions of the different strand materials are summarized in Table I.

### B. Thermal Treatments

Strand samples were examined before heat-treatment and after 24 h *ex-situ* heating at 170 °C, 220 °C, and after nine days 220 °C. In order to distinguish between the influence of Sn melting and intermetallics growth on the void formation, an additional sample was heated to 245 °C (just above the Sn melting temperature) for less than 10 min and afterwards the

Manuscript received July 3, 2006; revised September 1, 2006.
A. Haibel is with the Hahn-Meitner Institut Berlin (HMI), D-14109 Berlin, Germany.
C. Scheuerlein is with the European Organization for Nuclear Research (CERN), CH-1211, Geneva 23, Switzerland (e-mail: christian.scheuerlein@cern.ch).
Color versions of one or more of the figures in this paper are available online at http://ieeexplore.ieee.org.
Digital Object Identifier 10.1109/TASC.2006.887546

1051-8223/$25.00 © 2007 IEEE

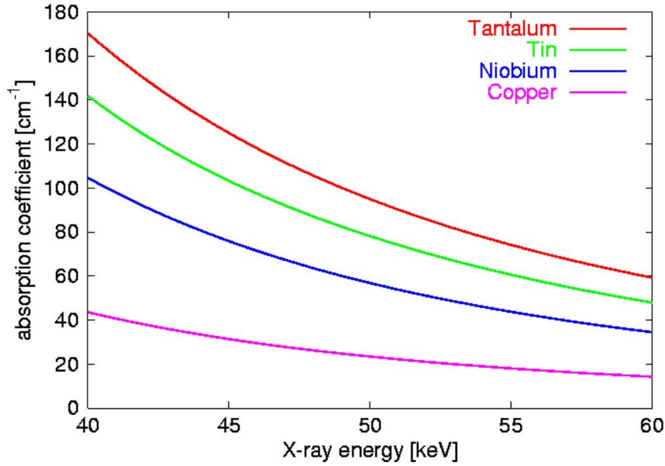


Fig. 1. Linear absorption coefficients of tantalum, tin, niobium, and copper. X-ray energy range used for the tomography experiments was 42–55 keV.

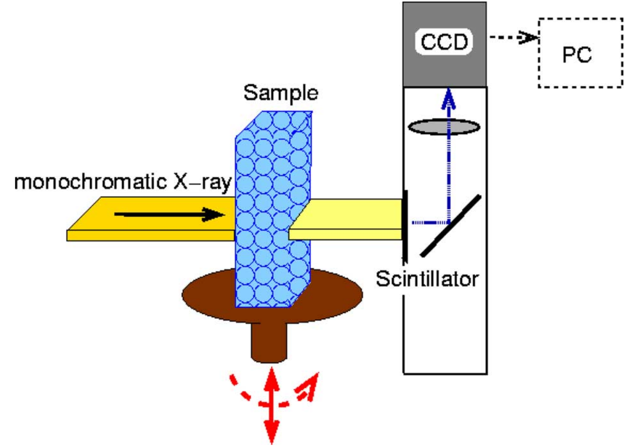


Fig. 2. Sketch of the tomographic setup.

temperature was kept constant at 220 °C for 24 h. In this way, two samples with similar intermetallics volume are produced in which in one case Sn has melted and in the other case Sn melting is avoided. In the following, the sample which was heated to a maximum temperature of 245 °C is referred to as "max. 245 °C."

The heating temperature has been measured with a thermocouple, which was in good thermal contact with the strand sample. The accuracy of the temperature measurements is estimated as $\pm 3$ °C and the temperature increase was $20°\mathrm{C}\ \mathrm{min}^{-1}$. The temperature reading during all heating cycles was recorded and did never exceed the adjusted temperature by more than 2 °C. At the end of the heating cycles, the samples were taken out of the furnace and quenched in water.

The ends of the strands were carefully closed by crimping in order to avoid leaking out of molten Sn during the heat treatments. After the heat treatments, the outer sample surface did not show any signs of Sn leakage. The heat treated strands were about 10 cm long and only the center part of these samples was analyzed.

### *C. Metallographic Sample Preparation*

For grinding and polishing of metallographic cross sections, the strand samples are mounted in a cold resin, assuring a perpendicular cut. Wet grinding is done using silicon carbide paper in three steps (360 grit, 600 grit, and finally 1000 grit). For sample polishing, 9- and 3-$\mu\mathrm{m}$ diamond particle suspensions are used. For the last polishing step, a 0.1-$\mu$m colloidal silica suspension with $\mathrm{pH} = 9$ is used (combined mechanical and chemical polishing). All grinding and polishing steps are done with complementary head direction and a sample force of about 15 N. The thickness of the damaged surface layer is estimated as 0.2 $\mu$m (two times the last polishing particle size).

### *D. Synchrotron Tomography*

Three-dimensional tomograms of about 2-mm-long strand sections have been reconstructed from the synchrotron absorption contrast, which depends on the average atomic number of the probed sample material (see Fig. 1) [5].

The tomography measurements were carried out at the beamline of the Federal Institute for Materials Research and Testing (BAM) at the electron synchrotron BESSY. The tomographic facility is run jointly by HMI and BAM and dedicated to the investigation of materials and compounds. By using a wave length shifter with a magnetic field of 7 T integrated into the storage ring, the measurement energy is tuneable from 6 to about 70 keV. The X-ray energy range used for the study of the $Nb_3Sn$ strand samples was 42–55 keV.

The parallel, highly intensive synchrotron radiation allows a high spatial resolution (depending on the used optics down to 1.5-$\mu$m pixel size), low number of artifacts and a very good signal-to-noise ratio. The beam was monochromized by a double multilayer monochromator with an energy resolution of about $10^{-2}$.

Fig. 2 shows a sketch of the tomographic setup. The monochromatic X-rays are attenuated by the sample followed by conversion into visible light by different kinds of scintillators. The choice of the scintillator depends on the X-ray energy and the required spatial resolution. In order to resolve the voids in the $Nb_3Sn$ strand samples, single crystal scintillators are required. For the measurements presented here, a new developed $\mathrm{CdWO_4}$ single crystal scintillator (20 $\mu$m layer) was used.

The radiographic images were magnified and projected on a Princeton Instruments camera with a charge-coupled device (CCD) chip of $2\mathrm{k} \times 2\mathrm{k}$ pixels. For the tomographic pictures 1200 radiographic images with an angle increment of 0.15° and an optical resolution of 1.5 $\mu$m were measured.

## III. Results

### *A. Synchrotron Absorption Tomography Versus Optical Metallography*

In Fig. 3, the cross section of a non-heat treated $Nb_3Sn$ strand reconstructed from the synchrotron absorption contrast is compared with the optical true color image of a metallographically prepared sample in order to demonstrate the potential of synchrotron tomography to resolve the different phases in internal tin $Nb_3Sn$ superconductors.

It can be seen that, apart from the Nb–Ta filaments, the strand geometry is correctly resolved in the tomogram. The separation

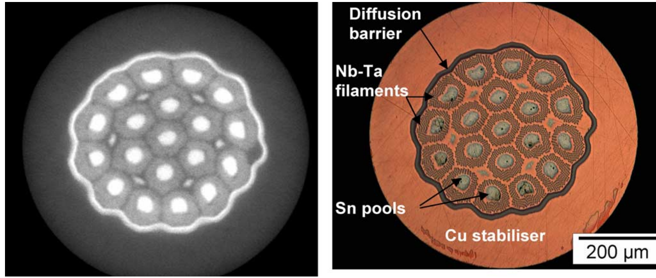


Fig. 3. Non-reacted $Nb_3Sn$ strand cross sections obtained by synchrotron tomography (left) and by optical metallography (right). Nb-Ta filaments appear as a blurred ring around the Sn diffusion centers because the spatial resolution of the tomography setup is not sufficient to resolve the filament separation of about 1 $\mu$m.

of the Nb–Ta filaments in the Cu matrix is smaller than the spatial resolution of the tomographic setup. Therefore, the Nb–Ta filaments appear as a blurred ring around the Sn reservoirs. In the non-reacted strand, voids are neither observed in the tomogram nor in the metallographic strand cross section.

## *B. Void Formation During Cu–Sn Mixing Heat Treatment*

*1) Observation of Intermetallics Growth by Optical Metallography:* In Fig. 4, the metallographic diffusion center cross sections are shown after different thermal treatments. The pure Sn in the non-heat treated strand section is successively transformed into the intermetallic phases $Cu_6Sn_5$ and $Cu_3Sn$, which are visible as dark grey ($Cu_3Sn$) and bright grey ($Cu_6Sn_5$) rings surrounding the diffusion centers.

The intermetallics growth kinetics at 220 °C has been determined by measuring the intermetallics thickness in metallographic wire cross sections. The $Cu_3Sn$ growth occurs with a nearly parabolic law, indicating that the intermetallics formation process is diffusion controlled. Apparent rate constants $k$ for the intermetallic layer growth, estimated from the layer thickness $x$ and the growth time $t$ according to $k = \Delta x^2/2t$, are $k_{Cu_3}Sn = 1.2 * 10^{-16}$ $m^2 \cdot s^{-1}$ and $k_{Cu_6Sn_5} = 6.9 * 10^{-17}$ $m^2 \cdot s^{-1}$. Literature values for layer growth at 215 °C are $7.55 * 10^{-17}$ $m^2 \cdot s^{-1}$ and $1.58 * 10^{-16}$ $m^2 \cdot s^{-1}$ for $Cu_3Sn$ and $Cu_6Sn_5$, respectively [6].

*2) Void Formation as Observed by Synchrotron Tomography:* Fig. 5 shows a 3-D view of the Sn pools and the diffusion barrier of a strand sample after heat treatment at a maximum temperature of about 245 °C. The outer part of the Sn pools is reacted with Cu to $Cu_3Sn$ and $Cu_5Sn_6$ and, therefore, this part appears as a bright ring around the dark center of pure Sn. The outside surface of the Sn pools has changed from the laminar appearance, which is developed during the wire drawing process, to a cauliflower like appearance as it is typical for the intermetallics formed during the heat treatment. The diffusion barrier surface has kept its laminar structure. Large pores can be seen in two Sn pool centers.

In Fig. 6, a 3-D view of the voids remaining in the strands after different *ex-situ* thermal treatments is presented. In the tomograms the superconductor material has been transparently depictured.

The total void volume as well as the average volume and aspect ratio of the individual voids in the differently heat treated

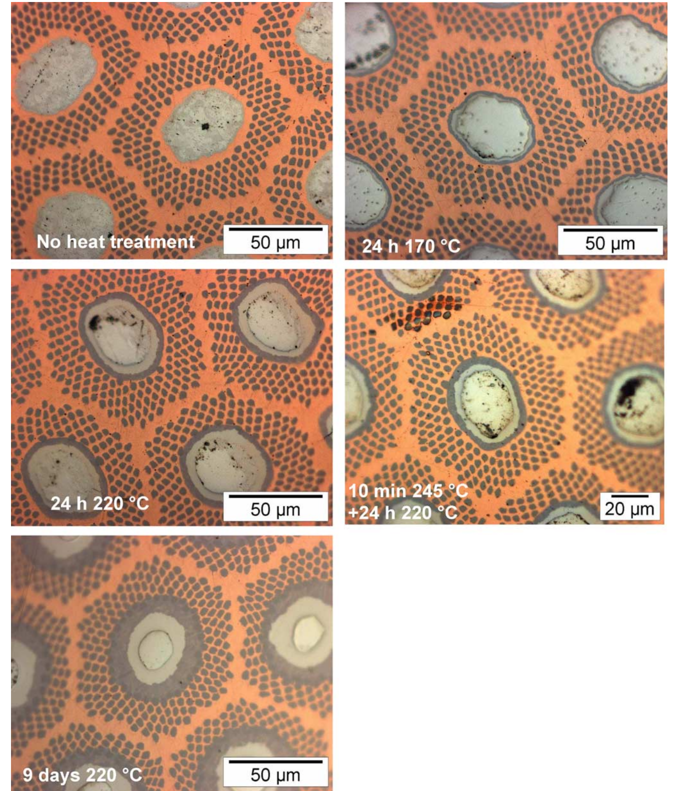


Fig. 4. Internal tin $Nb_3Sn$ strand cross sections obtained by optical metallography after different Cu–Sn mixing heat treatments. Pure Sn present in the diffusion centers of the non heat treated strand cross section (see also Fig. 3) is successively transformed into the intermetallic phases $Cu_6Sn_5$ (bright grey) and $Cu_3Sn$ (dark grey).

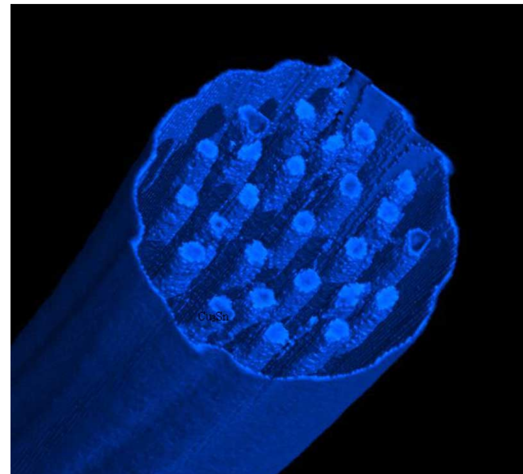

Fig. 5. Three-dimensional view of the diffusion barrier and Sn pools inside a strand sample after max. 245 °C heat treatment. Tomogram has been acquired in the center of a 10-cm-long sample.

strands is presented in Table II. Whereas in the non-heat treated sample, no voids are detected, after the 24 h-170 °C treatment relatively small pores with globular appearance are observed in the Sn pools. After the 24 h-220 °C heat treatment the total void volume is increased about tenfold with respect to the 170 °C heat treated sample. Further increasing the 220 °C heat treatment time does not significantly change the total void volume.

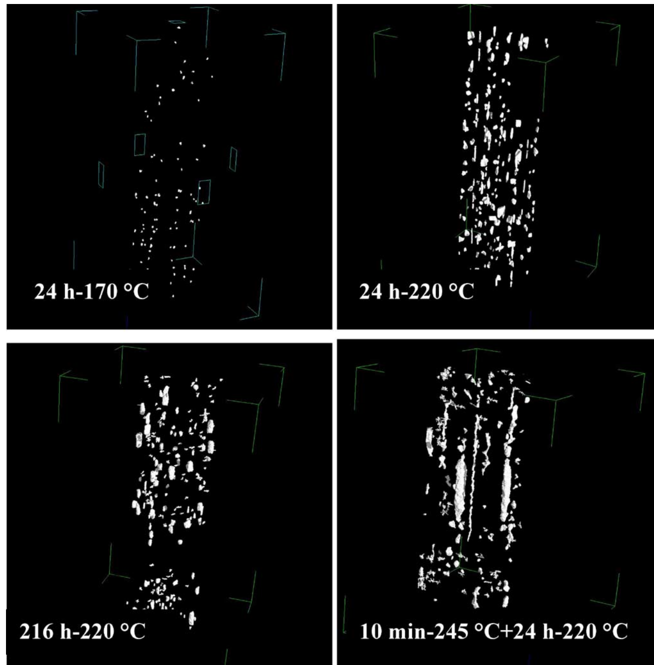


Fig. 6. 3-D view of the pores in the $Nb_3Sn$ strand after 24 h-170 °C, 24 h-220 °C, 216 h-220 °C, $10\ \mathrm{min} - 245°\mathrm{C} + 24\ \mathrm{h} - 220°\mathrm{C}$ heat treatment. Number of voids and their shape differs strongly after the different heat treatments, while there are only small differences in the total void volume for the samples heated to 220 °C and max. 245 °C.

TABLE II
NUMBER OF VOIDS PER $\mathrm{mm}^3$ SAMPLE VOLUME, AVERAGE VOLUME OF INDIVIDUAL VOIDS, AVERAGE VOID ASPECT RATIO (DEFINED AS THE MAXIMUM TO MINIMUM VOID DIAMETER RATIO), AND TOTAL VOLUME OF ALL VOIDS AS MEASURED BY SYNCHROTRON ABSORPTION TOMOGRAPHY FOR THE DIFFERENT *EX-SITU* HEAT TREATED SAMPLES

| *Heat treatment* | *No. of voids* | *Average void volume ($\mu m^3$)* | *Average void aspect ratio* | *Total void volume (% of strand volume)* |
|---|---|---|---|---|
| No HT | 0 | X | X | 0 |
| 24 h-170 °C | 207 | 324 | 4.1 | 0.0068 |
| 24 h-220 °C | 532 | 1460 | 17 | 0.085 |
| 216 h-220 °C | 677 | 1210 | 18 | 0.082 |
| Max. 245 °C +24 h- 220 °C | 427 | 2220 | 50 | 0.096 |

The shape and volume of the individual voids in the center of the Sn pools changes strongly when the Sn melting temperature has been exceeded. The total void volume is only slightly affected by the Sn melting.

## IV. DISCUSSION

### A. The Void Formation Mechanism

Possible mechanisms for the void formation in internal tin $Nb_3Sn$ strands include a partly plastic strand deformation during Sn volume changes upon melting and phase transformations, density changes due to the formation of intermetallics ($Cu_6Sn_5$ and $Cu_3Sn$), and nucleation and growth of voids as a result of differences in Sn and Cu diffusivities.

TABLE III
DENSITIES OF SOLID Cu, SOLID, AND LIQUID Sn, AND THE INTERMETALLIC PHASES FORMED INSIDE THE $Nb_3Sn$ STRAND DURING THE Cu–Sn MIXING HEAT TREATMENT UP TO 350 °C; ROOM TEMPERATURE DENSITIES OF THE INTERMETALLIC PHASES REPORTED IN [12] HAVE BEEN CALCULATED FROM PUBLISHED LATTICE PARAMETERS AND THE VALUES REPORTED IN [13] WERE MEASURED FOR $Cu_3Sn$ AND $Cu_6Sn_5$ SAMPLES

| *Phase* | *Density (g cm$^{-3}$)* | *Volume change with respect to pure β-Sn and Cu volume* |
|---|---|---|
| β-Sn | 7.26 [14] | 0 |
| γ-Sn | 6.60 [15] | +10 % |
| Liquid Sn | 6.97 [14] | + 5 % |
| Cu | 8.96 [14] | 0 |
| $Cu_6Sn_5$ | 8.27 [12]<br>8.28 [13]<br>(Cu*6+β-Sn*5)/11=8.19 | -1 % |
| $Cu_3Sn$ | 8.45 [12]<br>8.90 [13]<br>(Cu*3+β-Sn)/4=8.54 | +1 %<br>-4 % |

In order to assess the possible contribution of each of these mechanisms, the densities of the different phases that can be present in internal tin strands during the Cu–Sn mixing heat treatment up to 350 °C are summarized in Table III, together with the relative volume changes during phase transformations with respect to the volume of the pure solid $\beta$-Sn and Cu in their stoichiometric quantities.

For $Cu_6Sn_5$, there is good agreement between the measured and calculated density, indicating a volume decrease of about 1% upon the formation of $Cu_6Sn_5$ from Cu and $\beta$-Sn. For $Cu_3Sn$, there is a discrepancy between measured and calculated density values that have been reported. The calculated density indicates that the $Cu_3Sn$ volume is approximately 1% higher than the volume of the Cu and Sn from which it is formed.

*1) Volume Changes Upon the Formation of CuSn Intermetallics:* The intermetallics volume in the strand after 216 h-220°C heat treatment is more than twice the intermetallics volume after 24 h-220 °C treatment. If void growth would be caused by density changes upon formation of $Cu_6Sn_5$ and $Cu_3Sn$, one should expect that the void volume increases with the intermetallics volume. Since no influence of the 220 °C heating time on the void volume has been observed it is concluded that density changes due to the formation of CuSn intermetallics are not the main reason for the void growth.

*2) The Effect of Sn Melting:* A comparison of the total void volume in the strands after the different heat treatments (see Table II) shows that after resolidification of the liquefied Sn there is no strong void volume increase with respect to the void volume in the strands in which Sn was not melted before the 24 h-220 °C heat treatment. The main effect of the Sn melting is the strong change of the volume and shape of the individual voids, e.g., expressed in the average aspect ratio, as compared to the voids that are formed by heat treatments below the Sn melting temperature and subsequent cool down.

*3) Volume Changes Upon the Transformation of $\beta$-Sn to $\gamma$-Sn:* The existence of a third allotropic form of Sn, $\gamma$-Sn, is discussed controversially [7], [8] and its formation above

162 °C is supposed to depend on the Sn pressure. If $\beta$-Sn with a tetragonal lattice would be transformed into the brittle $\gamma$-Sn with a rhombic lattice, this would cause a strong volume expansion of about 10% (see Table III). Subsequent volume shrinkage when $\gamma$-Sn would be transformed back to $\beta$-Sn during cooling could possibly explain the presence of voids in the 170 °C and 220 °C heat treated strand samples.

*4) Are There Kirkendall Voids Formed During the 220 °C Heat Treatments?:* During the solid state Cu–Sn interdiffusion there is a generation of vacancies due to differences of the diffusion coefficients of Cu in Sn and Sn in Cu. Under certain conditions, the generation of vacancies can cause the nucleation and growth of voids, which are commonly referred to as Kirkendall voids [6]. Such voids occur for instance during the 200 °C heat treatment of the Sn coated Cu matrix of Nb–Ti superconducting strands, when Sn interdiffuses with the Cu strand matrix to form $Cu_3Sn$ [9].

In the present study of the internal tin $Nb_3Sn$ strand Kirkendall voids have not been observed in strand samples that were heat treated up to 245 °C. The reason for this apparent discrepancy might be that the voids are not formed because of the high pressure in the strands [10], or a lack of tensile stress that is necessary for the nucleation and growth of Kirkendall voids [3]. The formation of the relatively small voids distributed around the filaments, which are often referred to as Kirkendall voids, have been observed by synchrotron tomography after *ex-situ* heat treatment at 310 °C and at higher temperatures. The formation of these voids in internal tin design strands will be studied by *in-situ* synchrotron tomography and will be discussed in a further paper.

### B. Influence of Holding Steps

The Cu–Sn intermetallics growth rate at 162 °C is so low that Sn can not be transformed into intermetallics in a reasonable time scale below the reported $\beta$-Sn to $\gamma$-Sn transformation temperature. Holding temperatures below 162 °C are, therefore, not assumed to be useful for the suppression of voids inside pure Sn pools.

Sn melting may be avoided by holding steps below 232 °C. However, for the internal tin wire studied here it would take more than one month to transform the main Sn pools entirely into $Cu_6Sn_5$ and $Cu_3Sn$ at 220 °C. Hence, Sn melting in internal tin strands can be avoided only with strand designs where the Sn pool diameter is strongly reduced. In order to transform all Sn into $Cu_6Sn_5$ and $Cu_3Sn$ during a 24 h-220 °C holding step, the Sn pool diameter must not exceed about 6 $\mu$m. Avoiding the Sn melting would mainly influence the size and shape of individual voids rather than the total void volume.

### C. Potential of Synchrotron Tomography for the Characterization of $Nb_3Sn$ Superconductors

It has been demonstrated that synchrotron tomography allows the resolution of the voids formed during the reaction heat treatment of $Nb_3Sn$ superconductors. Thus, synchrotron tomography, in particular during *in-situ* heat treatments, is a helpful tool for obtaining a better understanding of the void formation mechanisms and the influence of different heat treatments and strand designs.

The irregular shape and distribution of the voids (see Fig. 6) is an intrinsic problem of metallographic studies of void growth. Depending on the longitudinal position at which the wire is cross sectioned, after identical heat treatments either large voids can be detected or no voids at all can be seen. Therefore, the influence of a certain heat treatment on void volume can only be assessed from 3-D images of the voids within a sufficiently large sample volume. In metallography, sample preparation artifacts may also obscure the voids, for instance by smearing the soft Sn over the less ductile adjacent metals during the mechanical sample grinding and polishing procedures. Such artifacts are excluded in synchrotron tomography.

Apart from the study of void growth, synchrotron tomography may also be useful for the examination of the strain induced crack formation in the brittle $Nb_3Sn$ phase of reacted strands. Conventional metallographic techniques have in this case the disadvantage that cracks in $Nb_3Sn$ may be induced even with the most sophisticated polishing procedures [11]. The dimensions of the cracks in $Nb_3Sn$ are in the order of 0.1 $\mu$m and, therefore, can not be resolved by synchrotron absorption tomography as it has been described here. However, phase contrast tomography may provide sufficient sensitivity for visualising these cracks and allow the observation of crack formation during *in-situ* straining of $Nb_3Sn$ strands.

## V. Conclusion

The tomography setup used clearly resolves the voids in the tin pools of internal tin process $Nb_3Sn$ strands. Unlike classical metallographic techniques, synchrotron tomography is nondestructive and can provide a quantitative description of the void volume, shape, and distribution within the strands.

The tomograms obtained after *ex-situ* thermal treatments show clearly that voids are already formed at temperatures below the Sn melting temperature of 232 °C. Sn melting and subsequent Sn shrinking during solidification does not cause a strong increase in the total void volume but changes strongly the volume and shape of individual voids.

The influence of temperature holding steps during the Cu–Sn mixing heat treatment on the void formation and the formation of the relatively small voids around the Nb–Ta filaments is subject for further studies by *in-situ* synchrotron absorption tomography.

## Acknowledgment

The authors would like to thank W. Treimer for proposing synchrotron tomography for the observation of voids. The authors would like to thank J. Schulz and P. Lee for stimulating discussions about void and crack formation in $Nb_3Sn$ superconductors. The authors would also like thank to H. Riesemeier and T. Wolk for technical support at the BAMline. The samples were kindly provided by Alstom-MSA.

## REFERENCES

[1] M. T. Naus, P. J. Lee, and D. C. Larbalestier, "The Interdiffusion of Cu and Sn in Internal Sn $Nb_3Sn$ Superconductors," *IEEE Trans. Appl. Supercond.*, vol. 10, no. 1, pp. 983–987, Mar. 2000.

[2] M. T. Naus, M. C. Jewell, P. J. Lee, and D. C. Larbalestier, "Lack of influence of the $Cu_3Sn$ mixing heat treatments on the superconducting properties of two high-Nb, int ernal-Sn $Nb_3Sn$ conductors," in *AIP Conf. Proc. 614B*, 2002, pp. 1016–1022.

[3] J. D. Verhoeven, A. Efron, E. D. Gibson, and C. C. Cheng, "Void formation in $Nb_3Sn - Cu$ superconducting wire produced by the external tin process," *J. Appl. Phys.*, vol. 59, no. 6, pp. 2105–2113, 1986.

[4] M. Durante, P. Bredy, A. Devred, R. Otmani, M. Reytier, T. Schild, and F. Trillaud, "Development of a $Nb_3Sn$ multifilamentary wire for accelerator magnet applications," *Physica C*, vol. 354, pp. 449–453, 2001.

[5] M. D. Michiel *et al.*, "Fast microtomography using high energy synchrotron radiation," *Rev. Sci. Instrum.*, vol. 76, p. 043702-1-7, 2005.

[6] A. Paul, "The Kirkendall effect in solid state diffusion," Ph.D. dissertation, Technische Univ. Eindhoven, Eindhoven, The Netherlands, 2004.

[7] R. Kubiak, "Evidence for the existence of the $\gamma$ form of tin," *J. Less-Common Metals*, vol. 116, pp. 307–311, 1986.

[8] *Gmelins Handbuch der anorganischen Chemie*. Weinheim, Germany: Verlag Chemie, 1971.

[9] C. Scheuerlein, P. Gasser, P. Jacob, D. Leroy, L. Oberli, and M. Taborelli, "The effect of CuSn intermetallics on the interstrand contact resistance in superconducting cables for the large hadron collider," *J. Appl. Phys.*, vol. 97, no. 3, p. 33909-1-7, 2005.

[10] J. D. Klein, G. Warshaw, N. Dudziak, S. F. Cogan, and R. M. Rose, "On the suppression of Kirkendall porosity in multifilamentary superconducting composites," *IEEE Trans. Magn.*, vol. 17, no. 1, pp. 380–382, Jan. 1981.

[11] M. C. Jewell, P. J. Lee, and D. C. Larbalestier, "The influence of $Nb_3Sn$ strand geometry on filament breakage under bend strain as revealed by metallography," *Supercond. Sci. Technol.*, vol. 16, pp. 1005–1011, 2000.

[12] G. Ghosh, "Elastic properties, hardness, and indentation fracture toughness of intermetallics relevant to electronic packaging," *J. Mater. Res.*, vol. 19, no. 5, pp. 1439–1454, 2004.

[13] H. P. R. Frederikse, R. J. Fields, and A. Feldman, "Thermal and electrical properties of copper-tin and nickel-tin intermetallics," *J. Appl. Phys.*, vol. 72, no. 7, pp. 2879–2882, 1992.

[14] *"Handbook of Chemistry and Physics,"* 76th ed. D. R. Lide, Ed., CRC, Boca Raton, FL, 1995.

[15] V. I. Khitrova, "Crystal structure of $\gamma$-Sn," *Sov. Phys. Crystallogr.*, vol. 33, no. 1, pp. 139–141, 1988.

**Astrid Haibel** , photograph and biography not available at the time of publication.

**Christian Scheuelein** , photograph and biography not available at the time of publication.